J. Fluid Mech. (2025), *vol.* 1012, R3, doi:10.1017/jfm.2025.10209

JFM RAPIDS

Revisiting the theory of van Driest: a general scaling law for the skin-friction coefficient of high-speed turbulent boundary layers

Zhiye Zhao[1] and **Lin Fu**[1,2]

[1]Department of Mechanical and Aerospace Engineering, The Hong Kong University of Science and Technology, Clear Water Bay, Kowloon, Hong Kong

[2]Department of Mathematics, The Hong Kong University of Science and Technology, Clear Water Bay, Kowloon, Hong Kong

Corresponding author: Lin Fu, linfu@ust.hk

(Received 28 February 2025; revised 12 April 2025; accepted 1 May 2025)

The skin-friction coefficient is a dimensionless quantity defined by the wall shear stress exerted on an object moving in a fluid, and it decreases as the Reynolds number increases for wall-bounded turbulent flows over a flat plate. In this work, a novel transformation, based on physical and asymptotic analyses, is proposed to map the skin-friction relation of high-speed turbulent boundary layers (TBLs) for air described by the ideal gas law to the incompressible skin-friction relation. Through this proposed approach, it has been confirmed theoretically that the transformed skin-friction coefficient $C_{f,i}$, and the transformed momentum-thickness Reynolds number $Re_{\theta,i}$ for compressible TBLs with and without heat transfer, follow a general scaling law that aligns precisely with the incompressible skin-friction scaling law, expressed as $(2/C_{f,i})^{1/2} \propto \ln Re_{\theta,i}$. Furthermore, the reliability of the skin-friction scaling law is validated by compressible TBLs with free-stream Mach number ranging from 0.5 to 14, friction Reynolds number ranging from 100 to 2400, and the wall-to-recovery temperature ratio ranging from 0.15 to 1.9. In all of these data, $(2/C_{f,i})^{1/2}$ and $\ln Re_{\theta,i}$ based on the present theory collapse to the incompressible relation, with a squared Pearson correlation coefficient reaching an impressive value 0.99, significantly exceeding 0.85 and 0.86 based on the established van Driest II and the Spalding–Chi transformations, respectively.

Key words: compressible boundary layers, turbulent boundary layers, turbulence theory

1. Introduction

The turbulent boundary layer (TBL) is among the most intriguing and important turbulent flows, drawing numerous researchers to engage in both physical and mathematical modelling of this phenomenon (Bradshaw 1977; Duan *et al.* 2010; Pirozzoli 2011; Smits *et al.* 2011; Marusic & Monty 2019; Chen *et al.* 2023; Cheng & Fu 2024). It is well known that incompressible TBLs at high Reynolds numbers exhibit several nearly universal scaling laws (van Driest 1951; Nagib *et al.* 2007; Marusic *et al.* 2013; Chen & Sreenivasan 2021). For example, the mean streamwise velocity profiles versus the wall-normal coordinate can be unified into the law of the wall through the non-dimensionalisation with respect to the friction velocity and kinematic viscosity. The skin-friction coefficient C_f decreases along the streamwise direction, and is widely recognised to exhibit a functional relation with the Reynolds number Re_θ based on the momentum thickness θ. The scaling law between C_f and Re_θ for incompressible TBLs over a flat plate can be expressed as (Nagib *et al.* 2007)

$$\left(\frac{2}{C_f}\right)^{1/2} \propto \ln Re_\theta, \tag{1.1}$$

as a result of the logarithmic law of the mean streamwise velocity.

However, the compressible TBLs with high free-stream Mach number and non-negligible heat transfer do not directly obey the above scaling laws observed in incompressible cases. Consequently, significant efforts are dedicated to mapping compressible TBLs onto the incompressible counterparts by considering variations in mean properties such as density and viscosity inspired by Morkovin hypothesis (Bradshaw 1977). Such a transformation holds not only theoretical significance but also practical importance for reduced-order turbulence modelling, since it would enable the established incompressible wall models to be seamlessly applied to compressible flows (Chen *et al.* 2024). An exemplary instance of the mapping is the velocity transformation. Over the past decades, several variants have been proposed for the velocity transformation of compressible TBLs (Zhang *et al.* 2012; Trettel & Larsson 2016; Volpiani *et al.* 2020*b*; Griffin *et al.* 2021; Hasan *et al.* 2023), building upon the pioneering work of van Driest (1951). Among these methods, the physics-based Griffin-Fu-Moin (GFM) transformation (Griffin *et al.* 2021) combining the modified transformation of Zhang *et al.* (2012) with the transformation of Trettel & Larsson (2016) successfully collapses mean streamwise velocity profiles of compressible TBLs with and without heat transfer into the law of the wall observed in incompressible scenarios.

In the field of aerospace engineering, it is essential to predict C_f on a surface where high-speed airflow passes along with intense heat transfer. To this end, there are approximately 30 published theories for calculation of C_f of compressible TBLs (Spalding & Chi 1963). The theories presented by van Driest (1951) and Spalding & Chi (1964) exhibit lowest root mean square error, and are two of the most commonly used models to estimate C_f. Specifically, considering variations in density and viscosity, van Driest (1951) introduced a scaling of C_f with Reynolds number for compressible TBLs, which can be reduced to the incompressible relation as the Mach number approaches zero and the heat transfer becomes negligible. According to Spalding & Chi (1964), the compressible scaling of C_f can be mapped to the incompressible relation by multiplying C_f and Re_θ by F_C and F_θ, respectively. Here, F_C and F_θ are functions of free-stream Mach number Ma_∞ and temperature T. Spalding & Chi (1964) formulated F_C and F_θ based on the theory of van Driest (1951), called the van Driest II (vD-II) transformation. Moreover, an empirically modified F_θ using C_f data in the presence of heat transfer is proposed as the Spalding–Chi (SC) transformation (Spalding & Chi 1964). Hopkins & Inouye (1971) compared the performance of the above two transformations, and concluded that neither theory provided accurate predictions of C_f for problems with wall-to-recovery temperature ratios below 0.3. The review by Bradshaw (1977) further remarked that these two theories failed to predict C_f on a very cold wall. In a more recent study, Huang *et al.* (2022) confirmed that neither of the two theories could map the compressible scaling of C_f to incompressible relation for a highly cooled wall.

Based on the aforementioned discussions, none of the theories could consistently predict the C_f of compressible TBLs with and without heat transfer. To this end, we revisit the theory of van Driest (1951), and introduce a novel transformation for C_f in this work. This proposed approach effectively maps the scaling law of C_f for high-speed TBLs in air described by the ideal gas law, particularly those involving highly cooled walls, to the incompressible relation (i.e. (1.1)).

2. Scaling law of C_f for compressible TBLs over a flat plate

The skin-friction coefficient, defined as $C_f = 2\tau_w/\rho_\infty u_\infty^2$ with wall shear stress $\tau_w = \overline{\mu}\, \mathrm{d}\overline{u}/\mathrm{d}y|_w$, free-stream density ρ_∞, free-stream velocity u_∞, viscosity $\overline{\mu}$ and wall-normal coordinate y, is a crucial parameter in the design of supersonic and hypersonic aircraft. Hereafter, an overline denotes the Reynolds average, and subscripts w and ∞ represent quantities at the wall and in the free stream, respectively. Coefficient C_f is widely recognised to exhibit a functional relation with the Reynolds number $Re_\theta = \rho_\infty u_\infty \theta/\mu_\infty$ based on the momentum thickness θ. According to Spalding & Chi (1964), for compressible TBLs over a flat plate, C_f and Re_θ can be linearly transformed to $C_{f,i}$ and $Re_{\theta,i}$ by multiplying by F_C and F_θ, respectively, i.e.

$$C_{f,i} = F_C C_f, \quad Re_{\theta,i} = F_\theta\, Re_\theta. \tag{2.1}$$

Here, $C_{f,i}$ and $Re_{\theta,i}$ should obey the incompressible scaling for C_f, i.e. (1.1). The transformation factor F_C is the same in both vD-II (van Driest 1951) and SC (Spalding & Chi 1964) theories considering variations in density and viscosity, and can be expressed as

$$(F_C)_{vD} = (F_C)_{SC} = \left[\int_0^1 \sqrt{\frac{\overline{\rho}}{\rho_\infty}}\, \mathrm{d}z\right]^{-2}, \tag{2.2}$$

with $z = \overline{u}/u_\infty$, density $\overline{\rho}$ and streamwise velocity $\overline{u}$. Here, subscripts 'vD' and 'SC' refer to the transformation factors from the vD-II and SC theories, respectively. Using the fact that the pressure is nearly constant in TBLs and the velocity–temperature relation, the factor F_C can be further written as

$$(F_C)_{vD} = (F_C)_{SC} = \frac{\dfrac{T_r}{T_\infty} - 1}{\left(\sin^{-1}\alpha + \sin^{-1}\beta\right)^2}, \tag{2.3}$$

where $\alpha = (2A^2 - B)/(B^2 + 4A^2)^{1/2}$, $\beta = B/(B^2 + 4A^2)^{1/2}$, $A = [r(\gamma - 1)/2 \times Ma_\infty^2\, T_\infty/T_w]^{1/2}$ and $B = T_r/T_w - 1$. Here, r is the recovery factor, T_r is the recovery temperature, and γ is the heat capacity ratio. However, the factor F_θ differs between the two theories and is given as

$$(F_\theta)_{vD} = \frac{\mu_\infty}{\mu_w}, \quad (F_\theta)_{SC} = \left(\frac{T_\infty}{T_w}\right)^{0.702}\left(\frac{T_r}{T_w}\right)^{0.772}. \tag{2.4}$$

These two transformations are used most commonly but fail to predict C_f on a highly cooled wall (Hopkins & Inouye 1971; Bradshaw 1977; Huang *et al.* 2022). The key issue with these two theories is the use of a linear transformation to eliminate the influences of Mach number and heat transfer on Re_θ. Indeed, the momentum thickness is defined as

$$\theta = \int_0^{\delta_e} \frac{\overline{\rho}}{\rho_\infty} \frac{\overline{u}}{u_\infty} \left(1 - \frac{\overline{u}}{u_\infty}\right) \mathrm{d}y, \tag{2.5}$$

where δ_e represents the TBL edge, typically chosen at the location where $\overline{u} = 0.99 u_\infty$. It is evident that the integrand in the definition of θ is a quadratic function of the velocity profile. Hence the factor F_θ in the linear transformation of (2.1) is unavailable to include all effects of Mach number and heat transfer on $\overline{u}$. To address this concern, we redefine a momentum thickness θ^* as

$$\theta^* = \int_0^{\delta_e} \frac{\overline{\rho}}{\rho_\infty} \frac{\overline{U}_I}{U_{I,\infty}} \left(1 - \frac{\overline{U}_I}{U_{I,\infty}}\right) \mathrm{d}(y^* \delta_v), \tag{2.6}$$

where δ_e is determined at $\overline{U}_I = 0.99 U_{I,\infty}$, the semi-local wall-normal coordinate is $y^* = y\sqrt{\tau_w \overline{\rho}}/\overline{\mu}$, the viscous length scale is $\delta_v = \mu_w/\sqrt{\tau_w \rho_w}$, and $\overline{U}_I$ using the physics-based GFM velocity transformation (Griffin *et al.* 2021) is given as

$$\overline{U}_I = \int_0^{y^*} \frac{\dfrac{1}{\overline{\mu}^+} \dfrac{\mathrm{d}\overline{U}^+}{\mathrm{d}y^*}}{1 + \dfrac{1}{\overline{\mu}^+} \dfrac{\mathrm{d}\overline{U}^+}{\mathrm{d}y^*} - \overline{\mu}^+ \dfrac{\mathrm{d}\overline{U}^+}{\mathrm{d}y^+}} \, \mathrm{d}y^*. \tag{2.7}$$

Throughout this paper, the superscript $+$ indicates a non-dimensionalisation by the friction velocity $u_\tau = \sqrt{\tau_w/\rho_w}$, δ_v and μ_w. Note that $\overline{U}_I$ in (2.7) is based on constant-stress-layer GFM transformation. In fact, the performances of $\overline{U}_I$ based on total-stress-based GFM transformation without the constant-stress-layer assumption, and on constant-stress-layer GFM transformation, are nearly identical (Griffin *et al.* 2021). Therefore, the constant-stress-layer assumption in (2.7) does not impact the establishment of the skin-friction scaling law, which has also been validated in Appendix A. The profiles of the transformed $\overline{U}_I(y^*)$ in compressible TBLs, with and without heat transfer, collapse to the incompressible law of the wall, and are independent of Mach number and heat transfer. Clearly, θ^* is similar to the traditional momentum thickness θ, except that θ^* is based on $\overline{U}_I$ and y^*. Since the profiles of $\overline{U}_I(y^*)$ are independent of Mach number and heat transfer, θ^* can be physically interpreted as a momentum thickness unaffected by the effects of Mach number and heat transfer in the velocity profiles of compressible TBLs. Therefore, only $\overline{\rho}$ in the redefined θ^* is affected by Mach number and heat transfer. These effects can be reasonably included in a linear transformation factor F_{θ^*} with a redefined Reynolds number $Re_{\theta^*} = \rho_\infty u_\infty \theta^*/\mu_\infty$. It is important to highlight that by multiplying y^* by δ_v in (2.6), Re_{θ^*} can be precisely reduced to the Re_θ of the incompressible case, where $\overline{\rho}$ and $\overline{\mu}$ are nearly constant.

Subsequently, we will theoretically derive the scaling law for C_f based on Re_{θ^*}. Given the fact that the contribution of the integrand to θ^* in both the viscous sublayer ($\overline{U}_I/U_{I,\infty} \to 0$) and outer layer ($\overline{U}_I/U_{I,\infty} \to 1$) is negligible, the log-law behaviour of $\overline{U}_I$, expressed as

$$y^* = \frac{\exp(\kappa \overline{U}_I)}{E}, \tag{2.8}$$

is suitably employed to approximate θ^*. Here, κ is the von Kármán constant, and E is a constant. By substituting (2.8) into (2.6), one can obtain

$$\theta^* = \frac{\kappa}{E}\delta_v U_{I,\infty} \int_0^1 \frac{\overline{\rho}}{\rho_\infty} Z(1-Z)\exp(\kappa U_{I,\infty} Z)\,\mathrm{d}Z, \tag{2.9}$$

where $Z = \overline{U}_I / U_{I,\infty}$. The integral term in above equation, $\int_0^1 (\overline{\rho}/\rho_\infty) Z(1-Z) \exp(\kappa U_{I,\infty} Z)\,\mathrm{d}Z = 1/(\kappa U_{I,\infty}) \int_0^1 (\overline{\rho}/\rho_\infty) Z(1-Z)\,\mathrm{d}\exp(\kappa U_{I,\infty} Z)$, can be integrated by parts and expressed as

$$\begin{aligned}
&\frac{1}{\kappa U_{I,\infty}} \int_0^1 \frac{\overline{\rho}}{\rho_\infty} Z(1-Z)\,\mathrm{d}\exp(\kappa U_{I,\infty} Z) \\
&= \frac{1}{\kappa U_{I,\infty}} \left\{ \left[\frac{\overline{\rho}}{\rho_\infty} Z(1-Z)\exp(\kappa U_{I,\infty} Z) \right]_0^1 - \int_0^1 \exp(\kappa U_{I,\infty} Z)\,\mathrm{d}\frac{\overline{\rho}}{\rho_\infty} Z(1-Z) \right\} \\
&= -\frac{1}{\kappa U_{I,\infty}} \int_0^1 \left[\frac{\overline{\rho}}{\rho_\infty}(1-2Z) - \frac{Z(1-Z)}{\rho_\infty}\frac{\mathrm{d}\rho}{\mathrm{d}Z} \right] \exp(\kappa U_{I,\infty} Z)\,\mathrm{d}Z.
\end{aligned} \tag{2.10}$$

Here, the term $[(\overline{\rho}/\rho_\infty) Z(1-Z)\exp(\kappa U_{I,\infty} Z)]_0^1$ represents the difference in values of $[(\overline{\rho}/\rho_\infty) Z(1-Z)\exp(\kappa U_{I,\infty} Z)]$ at the locations $Z=1$ and $Z=0$. Similarly, by repeatedly applying integration by parts to (2.10), (2.9) can be expressed as an asymptotic series of $1/\kappa U_{I,\infty}$ as

$$\begin{aligned}
\theta^* = \frac{\kappa}{E}\delta_v U_{I,\infty} \times \Bigg\{ & \frac{\exp(\kappa U_{I,\infty}) + \dfrac{1}{\rho_\infty^+}}{(\kappa U_{I,\infty})^2} \\
& + \frac{\left\{ \dfrac{\mathrm{d}}{\mathrm{d}Z}\left[\dfrac{\overline{\rho}}{\rho_\infty}(1-2Z) - \dfrac{Z(1-Z)}{\rho_\infty}\dfrac{\mathrm{d}\rho}{\mathrm{d}Z} \right] \exp(\kappa U_{I,\infty} Z) \right\}_0^1}{(\kappa U_{I,\infty})^3} + O\left[\frac{1}{(\kappa U_{I,\infty})^4} \right] \Bigg\}.
\end{aligned} \tag{2.11}$$

According to the logarithmic law of TBLs, it can be estimated that $U_{I,\infty} \gtrsim 20$, leading to $\kappa U_{I,\infty}$ being of the order of $O(10)$ for TBLs. The ratio of magnitude of the third-order term related to $1/(\kappa U_{I,\infty})^3$ to the magnitude of the second-order term related to $1/(\kappa U_{I,\infty})^2$ is of the order of $O(10^{-1})$. Moreover, given the fact that pressure is nearly constant in TBLs, $1/\rho_\infty^+ \approx T_\infty / T_w$. For common high-speed TBLs, $T_\infty / T_w < 1$, which implies $1/\rho_\infty^+ < 1 \ll \exp(\kappa U_{I,\infty}) \sim O(10^4)$. To this end, the term $1/\rho_\infty^+$, which is much smaller than $\exp(\kappa U_{I,\infty})$, along with the higher-order terms that are smaller than the second-order term, can be neglected. Consequently, Re_{θ^*} can be determined by

$$Re_{\theta^*} = \frac{1}{E} \frac{\rho_\infty u_\infty \mu_w}{\mu_\infty \sqrt{\tau_w \rho_w}} \frac{\exp(\kappa U_{I,\infty})}{\kappa U_{I,\infty}}. \tag{2.12}$$

Moreover, according to (2.7), $U_{I,\infty}$ is determined by

$$U_{I,\infty} = \frac{u_\infty}{\sqrt{\dfrac{\tau_w}{\rho_w}}} \int_0^1 \frac{1}{\overline{\mu}^+ + \dfrac{\mathrm{d}\overline{U}^+}{\mathrm{d}y^*} - (\overline{\mu}^+)^2 \dfrac{\mathrm{d}\overline{U}^+}{\mathrm{d}y^+}} \,\mathrm{d}z. \tag{2.13}$$

Letting $F = \int_0^1 [\overline{\mu}^+ + \mathrm{d}\overline{U}^+/\mathrm{d}y^* - (\overline{\mu}^+)^2\, \mathrm{d}\overline{U}^+/\mathrm{d}y^+]^{-1}\,\mathrm{d}z$, which is determined by given viscosity and velocity profiles in TBLs, the functional relation between Re_{θ^*} and C_f can be obtained by substituting (2.13) into (2.12) as

$$\sqrt{\frac{2}{C_f \left(\dfrac{\rho_\infty}{\rho_w}\right) F^{-2}}} = \frac{1}{\kappa} \ln\left(\frac{\rho_w \mu_\infty}{\rho_\infty \mu_w} F\, Re_{\theta^*}\right) + C, \tag{2.14}$$

with a constant $C = \ln(E\kappa)/\kappa$. Obviously, we can define a novel transformation for C_f and Re_{θ^*} as

$$C_{f,i} = F_{C^*} C_f, \quad Re_{\theta,i} = F_{\theta^*}\, Re_{\theta^*}, \tag{2.15}$$

where the new transformation factors are expressed as

$$F_{C^*} = \frac{\rho_\infty}{\rho_w} F^{-2}, \quad F_{\theta^*} = \frac{\rho_w \mu_\infty}{\rho_\infty \mu_w} F. \tag{2.16}$$

Employing the present transformation, i.e. (2.15), the scaling for C_f of a compressible TBL can be written as

$$\left(\frac{2}{C_{f,i}}\right)^{1/2} \propto \ln Re_{\theta,i}. \tag{2.17}$$

The functional relation between the newly transformed $C_{f,i}$ and $Re_{\theta,i}$ is exactly the same as the incompressible scaling for C_f expressed by (1.1). Furthermore, in the incompressible TBL with constant $\overline{\rho}$ and $\overline{\mu}$, it is clear that $F_{C^*} = 1$, $F_{\theta^*} = 1$ and $Re_{\theta^*} = Re_\theta$. Hence the newly transformed $C_{f,i}$ and $Re_{\theta,i}$ can be precisely reduced to the incompressible counterparts when the effects of Mach number and heat transfer are negligible. The preceding discussions on the innovative transformation indicate that this novel approach theoretically maps the scaling for C_f of compressible TBLs for air described by the ideal gas law to the incompressible relation for C_f. Furthermore, by performing a linear fit of the data to determine the constants κ_f and C, the scaling for C_f of a compressible TBL can be quantified as

$$\left(\frac{2}{C_{f,i}}\right)^{1/2} = \frac{1}{\kappa_f} \ln Re_{\theta,i} + C. \tag{2.18}$$

Given the approximations involved in deriving the skin-friction scaling, the constant obtained by linearly fitting $(2/C_{f,i})^{1/2}$ and $\ln Re_{\theta,i}$ in (2.18) will differ from the value of the von Kármán constant κ obtained from the stream velocity profile, and is therefore denoted as κ_f. Additionally, based on the definition of Re_{θ^*}, the newly transformed $Re_{\theta,i}$ can be further expressed as $Re_{\theta,i} = F \rho_w u_\infty \theta^*/\mu_w$. It is evident that μ_∞ used in the present definition of Re_{θ^*} does not appear in the final form of transformed $Re_{\theta,i}$. In other words, in the definition of Re_{θ^*}, replacing μ_∞ with μ_w, shear stress-weighted average viscosity introduced by Kianfar *et al.* (2023) to account for the relative influence of turbulence on the skin friction, or any other viscosity, does not change the final form of the transformed $Re_{\theta,i}$.

Case	Ma_∞	T_w/T_r	Re_τ	Re_{δ_e}	Re_θ	Re_{θ^*}	$C_f \times 10^3$
Present DNS	4.0	0.5	664–790	48 769–59 273	3051–3649	7005–8312	1.96–1.88
	4.0	0.25	620–745	16 434–20 571	1223–1545	1062–1317	2.59–2.39
	6.0	0.5	748–814	227 507–249 253	9628–10 427	88 090–94 805	1.14–1.13

Table 1. The parameters for compressible TBLs self-simulated using the open-source code STREAmS (Bernardini *et al.* 2021, 2023) in fully developed turbulent regions. Here, Ma_∞ is the free-stream Mach number, T_w/T_r is the wall-to-recovery temperature ratio, Re_τ is the friction Reynolds number, Re_{δ_e} is the Reynolds number based on boundary layer thickness, Re_θ is the Reynolds number based on momentum thickness, and Re_{θ^*} is the redefined Reynolds number based on transformed momentum thickness.

Reference	Ma_∞	T_w/T_r	Re_τ	Re_{δ_e}	Re_θ	Re_{θ^*}	$C_f \times 10^3$
Zhang	0.5	1.0	563–696	13 552–17 433	1 426–1 862	1 509–1 967	3.86–3.56
et al.	2.0	1.0	661–820	36 532–47 060	2 945–3 815	5 892–7 592	2.59–2.40
(2022,	2.0	0.5	652–806	12 481–16 014	1 253–1 598	967–1 230	3.59–3.33
2024)	4.0	1.0	623–747	121 667–148 933	6 339–7 638	34 598–41 401	1.37–1.32
	6.0	1.0	589–702	519 256–629 102	18 517–22 041	449 876–528 268	0.79–0.77
	8.0	1.0	566–655	1 204 449–1 426 517	32 616–38 621	1 587 255–1 813 217	0.49–0.47
	8.0	0.5	601–710	460 813–555 324	15 484–18 265	305 564–355 140	0.71–0.68
Li *et al.*	2.25	1.0	607–776	38 962–52 592	2 760–3 913	6 398–9 038	2.61–2.35
(2009,	8.0	0.81	700–1175	660 259–1 200 648	17 476–34 771	313 120–561 846	0.51–0.44
2019)	8.0	0.15	1439–2271	154 565–259 128	5 907–10 597	13 465–21 977	0.88–0.78
Volpiani	2.28	1.0	246–280	14 196–16 598	1 126–1 320	2 532–2 965	3.03–2.86
et al.	2.28	1.0	410–491	25 406–31 555	1 987–2 493	4 456–5 596	2.63–2.45
(2018,	2.28	1.9	102–125	13 625–17 572	859–1 113	4 742–6 032	2.76–2.50
2020*a*)	5.0	0.8	691–795	174 578–210 194	7 263–9 186	45 980–56 792	1.19–1.08
	5.0	0.8	567–629	138 653–160 991	5 834–7 046	37 457–44 339	1.26–1.15
	5.0	1.9	188–206	149 146–171 344	4 643–5 591	100 185–116 561	1.02–0.93

Table 2. The parameters for compressible TBLs of Zhang *et al.* (2022, 2024), Li *et al.* (2009, 2019) and Volpiani *et al.* (2018, 2020*a*) in fully developed turbulent regions. The representations of the parameters are presented in table 1.

3. Validation of the newly proposed scaling law

To verify the scaling law for C_f, we conduct direct numerical simulations (DNS) of compressible TBLs, and also collect as much published DNS data as possible on compressible TBLs with adiabatic (Li *et al.* 2009; Pirozzoli & Bernardini 2011; Volpiani *et al.* 2018; Zhang *et al.* 2018, 2024; Maeyama & Kawai 2023; Cogo *et al.* 2023), cooled (Zhang *et al.* 2018, 2022; Li *et al.* 2019; Volpiani *et al.* 2020*a*; Cogo *et al.* 2023), and heated (Volpiani *et al.* 2018, 2020*a*) walls. The data cover a fairly wide range of flow conditions, with Ma_∞ ranging from 0.5 to 14, friction Reynolds number Re_τ ranging from 100 to 2400, and T_w/T_r ranging from 0.15 to 1.9. A wall-to-recovery temperature ratio T_w/T_r less than 1 signifies a cooled wall, T_w/T_r equal to 1 denotes an adiabatic wall, and T_w/T_r greater than 1 indicates a heated wall. Detailed parameters regarding the DNS data of TBLs can be found in tables 1, 2 and 3.

Figure 1(*a*) displays the correlation between the transformed $(2/C_{f,i})^{1/2}$ and $Re_{\theta,i}$ according to the proposed theory, employing logarithmic coordinate for $Re_{\theta,i}$. It should be noted that a second-order difference scheme is uniformly employed to calculate the

https://doi.org/10.1017/jfm.2025.10209 Published online by Cambridge University Press

Reference	Ma_∞	T_w/T_r	Re_τ	Re_{δ_e}	Re_θ	$Re_{\theta*}$	$C_f \times 10^3$
Maeyama & Kawai (2023)	2.28	0.96	716	45 005	3 466	7 463	2.36
	2.28	0.96	1279	86 515	6 440	14 082	2.06
	2.28	0.96	2405	171 960	12 296	27 131	1.84
Zhang *et al.* (2018)	2.50	1.0	505	36 942	2 694	6 508	2.30
	5.84	0.25	436	37 367	2 011	4 310	1.69
	5.86	0.76	448	240 290	9 583	129 938	0.96
	7.87	0.48	467	313 170	10 729	161 282	0.77
	13.64	0.18	634	701 422	17 689	204 479	0.39
Cogo *et al.* (2023)	2.0	1.0	444	23 633	1 981	3 900	2.81
	2.0	0.90	443	19 971	1 714	2 934	2.99
	2.0	0.79	443	16 609	1 486	2 159	3.17
	2.0	0.76	1947	87 859	7 954	11 581	2.16
	2.0	0.69	444	13 399	1 242	1 494	3.39
	4.0	0.81	444	63 551	3 657	14 604	1.63
	4.0	0.63	444	44 215	2 749	7 976	1.85
	4.0	0.44	444	27 001	1 848	3 428	2.15
	6.0	1.0	444	228 481	8 401	88 891	0.84
	6.0	0.78	444	166 073	6 643	53 030	0.94
	5.86	0.76	1947	996 276	41 172	410 017	0.69
	6.0	0.57	444	108 382	4 841	25 836	1.09
	6.0	0.35	444	56 610	2 813	8 531	1.34
Pirozzoli & Bernardini (2011)	2.0	1.0	204	10 216	877	1 793	3.45
	2.0	1.0	251	13 012	1 131	2 301	3.22
	2.0	1.0	445	24 792	2 090	4 276	2.79
	2.0	1.0	580	33 702	2 890	5 864	2.56
	2.0	1.0	838	51 312	4 437	9 092	2.30
	2.0	1.0	893	55 170	4 760	9 739	2.27
	2.0	1.0	992	62 125	5 347	10 938	2.21
	2.0	1.0	1106	70 513	6 045	12 325	2.13
	3.0	1.0	403	44 654	3 013	10 547	2.01
	3.0	1.0	502	57 893	3 955	13 606	1.86
	4.0	1.0	395	83 623	4 713	26 874	1.39
	4.0	1.0	501	107 715	5 943	33 392	1.34

Table 3. The parameters for compressible TBLs of Maeyama & Kawai (2023), Zhang *et al.* (2018), Cogo *et al.* (2023) and Pirozzoli & Bernardini (2011) in fully developed turbulent regions. The representations of the parameters are presented in table 1.

derivatives in F_{C^*} and F_{θ^*} for all data. With a squared Pearson correlation coefficient R^2 as high as 0.99 between $(2/C_{f,i})^{1/2}$ and $\ln Re_{\theta,i}$, it is indicated that the transformed $C_{f,i}$ of compressible TBLs with and without heat transfer strictly satisfies the incompressible scaling for C_f, i.e. $(2/C_{f,i})^{1/2} \propto \ln Re_{\theta,i}$, based on present theory. For comparison, the results of vD-II and SC theories are depicted in figures 1(*b*) and 1(*c*), respectively. No significant linear relationship is observed between $(2/C_{f,i})^{1/2}$ and $\ln Re_{\theta,i}$ under these two theories, with R^2 values 0.85 and 0.86, much less than 0.99 of present theory.

To quantitatively confirm if the present theory effectively collapses the compressible scaling for C_f to the incompressible relation, the constants κ_f and C are determined by linearly fitting present data for compressible TBLs, and (2.18) is plotted in figure 1. Two commonly used incompressible correlations for C_f, namely the modified Coles–Fernholz (Nagib *et al.* 2007) and Smits *et al.* (1983) relations, are also depicted. It is evident that the $C_{f,i}$ correlation of present theory lies between two incompressible relations at $Re_{\theta,i} \gtrsim 500$. However, the $C_{f,i}$ correlation of vD-II theory deviates from two incompressible relations at $Re_{\theta,i} \lesssim 10\,000$, and that of SC theory notably deviates

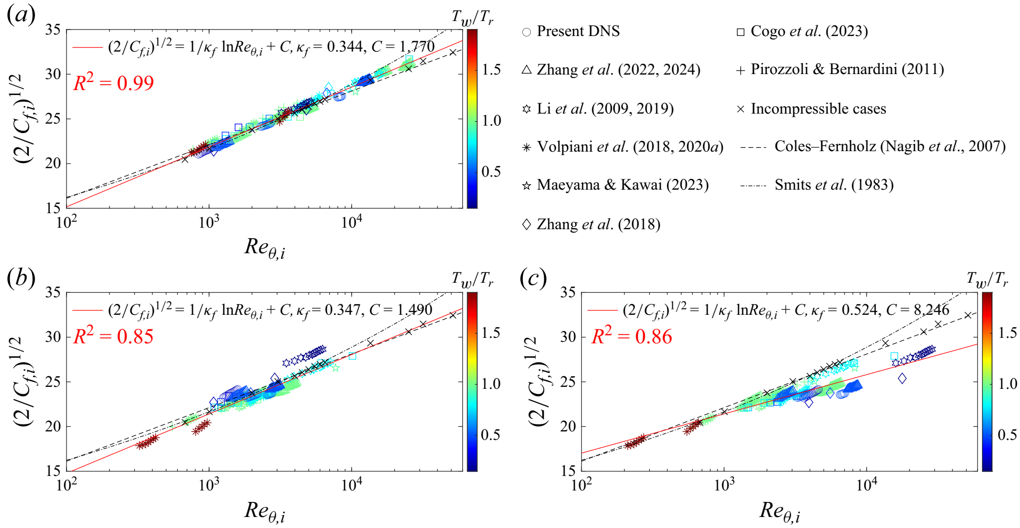

Figure 1. The transformed $(2/C_{f,i})^{1/2}$ versus transformed $Re_{\theta,i}$: (*a*) present theory (using (2.15)), (*b*) vD-II theory (using (2.1) with $(F_C)_{vD}$ and $(F_\theta)_{vD}$) and (c) SC theory (using (2.1) with $(F_C)_{SC}$ and $(F_\theta)_{SC}$). The coloured symbols represent DNS data from both adiabatic and diabatic compressible TBLs, with colours indicating the wall-to-recovery temperature ratios. The black symbols $\times$ denote DNS and experimental data for incompressible TBLs, with $Re_\theta \leqslant 3000$ from Schlatter & Örlü (2010), $4000 \leqslant Re_\theta \leqslant 6500$ from Sillero *et al.* (2013), and $13\,000 < Re_\theta < 52\,000$ (corresponding to $6000 < Re_\tau < 20\,000$) from Samie *et al.* (2018). The dashed and dash-dotted lines represent the incompressible correlations of Coles–Fernholz (modified by Nagib *et al.* (2007), i.e. $(2/C_{f,i})^{1/2}_{CF} = 2.604 \ln Re_{\theta,i} + 4.127$) and Smits *et al.* (1983) (i.e. $(C_{f,i})_{SM} = 0.024\, Re_{\theta,i}^{-1/4}$), respectively. The squared Pearson correlation coefficient R^2 between $(2/C_{f,i})^{1/2}$ and $\ln Re_{\theta,i}$ for each transformation is provided in each plot. For a pair of variables (X, Y), R^2 is defined as $R^2 = \mathrm{cov}^2(X, Y)/(\sigma_X^2 \sigma_Y^2)$, where cov denotes the covariance, σ_X is the standard deviation of X, and σ_Y is the standard deviation of Y.

from incompressible relations. Moreover, the C_f of incompressible DNS data (Schlatter & Örlü 2010; Sillero *et al.* 2013) and experimental data (Samie *et al.* 2018) also falls between two incompressible relations, following the $C_{f,i}$ correlation of present theory. Hence comparing with vD-II and SC theories, the present theory elegantly maps the compressible scaling for C_f to the incompressible relation. Additionally, the performance of present theory for TBLs at supercritical pressure is discussed in Appendix B.

Error statistics of $C_{f,i}$ from DNS data, compared to the modified Coles–Fernholz relation (Nagib *et al.* 2007), are provided in figure 2 to assess the theory's performance in predicting C_f for compressible TBLs. The maximum errors for the present, vD-II and SC theories are slightly below 5 %, slightly below 10 %, and surpassing 14 %, respectively. The data from compressible TBLs with heated and extensively cooled walls exhibit a significant error for vD-II theory, aligning with observations on the vD-II theory's inadequacy in predicting C_f on a highly cooled wall (Hopkins & Inouye 1971; Bradshaw 1977; Huang *et al.* 2022). The significant error in the SC theory indicates a notable deviation from incompressible relations, leading to its failure in predicting C_f of compressible TBLs. Therefore, the present theory provides the most reliable predictions of C_f for compressible TBLs with and without heat transfer.

The distributions of $C_{f,i}$ versus $Re_{\theta,i}$ are depicted directly in figure 3. Both compressible and incompressible data collapse to the $C_{f,i}$ correlation of the present theory, lying between two incompressible relations. Additionally, $C_{f,i}$ exhibits a typical

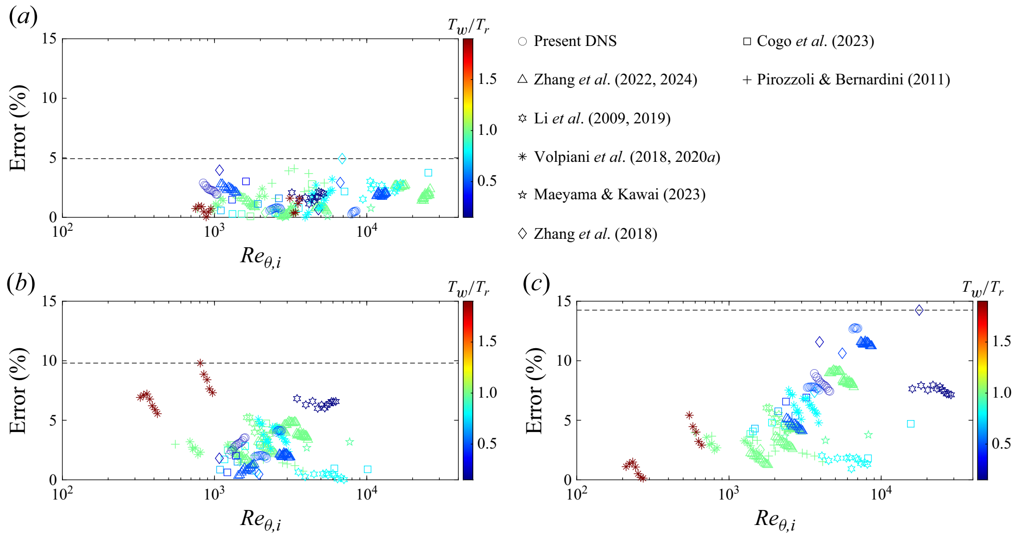

Figure 2. The error of the skin-friction coefficient, defined as $|(2/C_{f,i})^{1/2}_{DNS} - (2/C_{f,i})^{1/2}_{CF}|/(2/C_{f,i})^{1/2}_{CF}$: (*a*) present theory, (*b*) vD-II theory, and (*c*) SC theory. The black dashed line in each plot represents the maximum error.

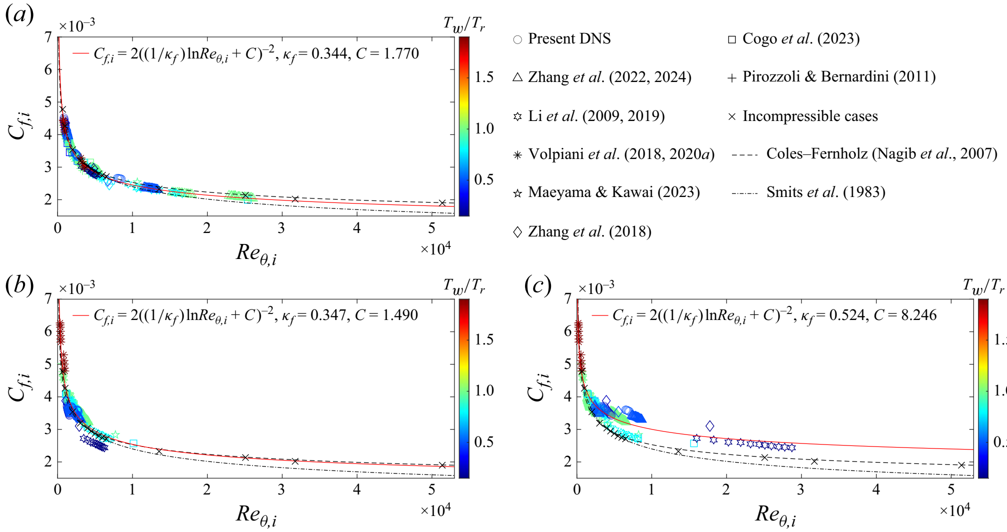

Figure 3. The transformed $C_{f,i}$ versus transformed $Re_{\theta,i}$: (*a*) present theory, (*b*) vD-II theory, and (*c*) SC theory.

decreasing relation with increasing $Re_{\theta,i}$. In the vD-II and SC theories, the data fail to collapse to their $C_{f,i}$ correlation. The $C_{f,i}$ of a highly cooled wall ($T_w/T_r \lesssim 0.3$) is overestimated by the vD-II theory but underestimated by the SC theory. This phenomenon is also noted by Huang *et al.* (2022). These observations further suggest that the newly proposed theory effectively unifies the compressible and incompressible scaling of C_f.

4. Conclusions

By redefining the Reynolds number, i.e. $Re_{\theta*}$, the defects of vD-II and SC transformations of C_f that do not completely absorb the effects of Mach number and heat transfer in high-speed TBLs for air described by the ideal gas law are overcome. Based on physical and asymptotic analyses, we derived a novel transformation utilising $Re_{\theta*}$ to precisely map the compressible scaling law for C_f to the incompressible relation, expressed as $(2/C_{f,i})^{1/2} \propto \ln Re_{\theta,i}$. Moreover, the transformed $C_{f,i}$ and $Re_{\theta,i}$ can be precisely reduced to the incompressible skin-friction coefficient and the Reynolds number when the effects of Mach number and heat transfer are negligible. By employing the novel theory, the transformed $C_{f,i}$ from the data of compressible TBLs over a flat plate with a fairly wide range of flow conditions elegantly collapses to the incompressible scaling law of C_f. Therefore, the newly established theory effectively unifies the scaling law for C_f in high-speed TBLs, both with and without heat transfer, and in incompressible TBLs.

Since the GFM transformation used to derive the scaling law is effective only for TBLs with air described by the ideal gas law over smooth flat plates with zero-pressure gradient, the present skin-friction scaling law is limited to these specific conditions. However, redefining $Re_{\theta*}$ to establish the skin-friction scaling law in the present study is enlightening. Future investigations can establish skin-friction scaling laws for TBLs with pressure gradients, surface roughness, supercritical pressure, or non-air-like viscosity law, utilising $Re_{\theta*}$ in conjunction with an appropriate velocity transformation. Moreover, the skin-friction scaling law established in the present work is of practical value. Specifically, the present skin-friction scaling law, validated by extensive DNS data, can serve as a reference for assessing the accuracy of methods that employ turbulence models, such as large eddy simulation and Reynolds-averaged Navier–Stokes methods, in simulating high-speed TBLs. Since the present method unifies the skin-friction scaling relations of compressible and incompressible TBLs, the C_f of high-speed TBLs can be obtained using results from incompressible flows at the same $Re_{\theta,i}$.

Acknowledgements. The authors express their gratitude to Dr P.-J.-Y. Zhang from the University of Science and Technology of China for providing the data.

Funding. This work was supported by the National Natural Science Foundation of China (nos 12388101, 12202436 and 12422210). L.F. also acknowledges the fund from the Research Grants Council (RGC) of the Government of Hong Kong Special Administrative Region (HKSAR) with RGC/ECS Project (no. 26200222), RGC/GRF Project (no. 16201023) and RGC/STG Project (no. STG2/E-605/23-N).

Declaration of interests. The authors report no conflict of interest.

Data availability statement. The data that support the findings of this study are available from the corresponding author upon reasonable request.

Appendix A

The performance of skin-friction transformation using $\overline{U}_I$, based on total-stress-based GFM transformation without constant-stress-layer assumption, is examined. The $\overline{U}_I$ for total-stress-based GFM transformation is expressed as

$$\overline{U}_I = \int_0^{y^*} \frac{\dfrac{\tau^+}{\overline{\mu}^+}\dfrac{\mathrm{d}\overline{U}^+}{\mathrm{d}y^*}}{\tau^+ + \dfrac{1}{\overline{\mu}^+}\dfrac{\mathrm{d}\overline{U}^+}{\mathrm{d}y^*} - \overline{\mu}^+\dfrac{\mathrm{d}\overline{U}^+}{\mathrm{d}y^+}}\,\mathrm{d}y^*, \tag{A1}$$

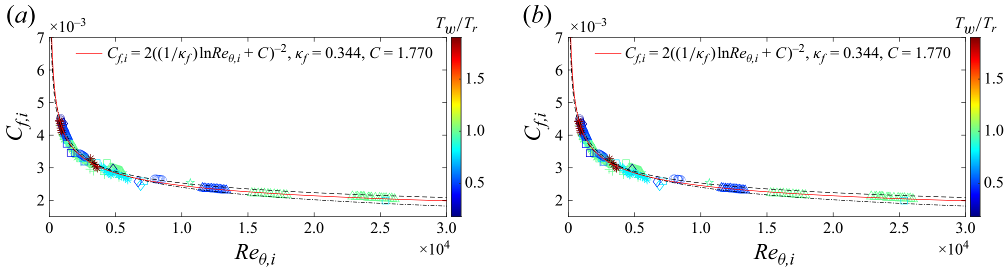

Figure 4. The transformed $C_{f,i}$ versus transformed $Re_{\theta,i}$ using $\overline{U}_I$ based on (*a*) constant-stress-layer GFM transformation and (*b*) total-stress-based GFM transformation.

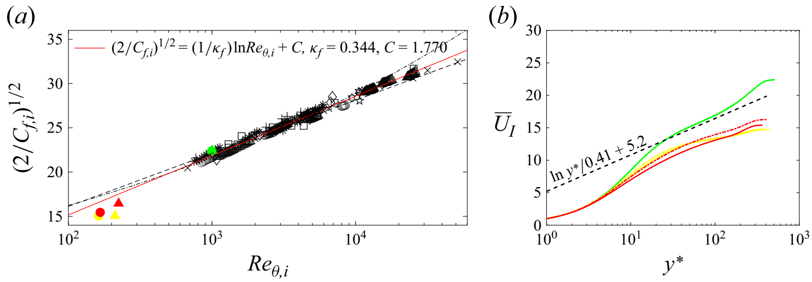

Figure 5. (*a*) Transformed $(2/C_{f,i})^{1/2}$ versus transformed $Re_{\theta,i}$ for the present theory. (*b*) Transformed stream velocity $\overline{U}_I$ using GFM transformation. Here, the filled coloured symbols and coloured lines represent data from TBLs at supercritical pressure with $Ma_\infty = 0.3$, as reported in Kawai (2019). The filled circle and triangle correspond to flows with free-stream pressures $p_\infty = 2$ and 4 MPa, respectively. The solid and dash-dotted lines represent flows at these same pressures. The colours green, yellow and red denote the temperature ratios $T_w/T_\infty = 1$, 4 and 8, respectively.

where τ^+ is the total shear stress (i.e. the sum of the viscous and Reynolds shear stresses) normalised by τ_w. Using (A1) to define $Re_{\theta*}$ does not alter the form of the transformation factors, except for $F = \int_0^1 \tau^+/[\tau^+\overline{\mu}^+ + \mathrm{d}\overline{U}^+/\mathrm{d}y^* - (\overline{\mu}^+)^2\, \mathrm{d}\overline{U}^+/\mathrm{d}y^+]\,\mathrm{d}z$ in F_{C*} and $F_{\theta*}$. Figure 4, which includes all DNS data providing total shear stress, illustrates the skin-friction scaling between transformed $C_{f,i}$ and $Re_{\theta,i}$ using $\overline{U}_I$ based on both constant-stress-layer GFM transformation and total-stress-based GFM transformation. Evidently, the constant-stress-layer assumption has little effect on the performance of the proposed skin-friction transformation.

Appendix B

Figure 5(*a*) illustrates the performance of the present skin-friction transformation on the data for TBLs at supercritical pressure from Kawai (2019). The transformed $C_{f,i}$ for TBLs at supercritical pressure with $T_w/T_\infty = 1$ obeys the proposed skin-friction scaling law, exhibiting an error of 1.3 %. In contrast, $C_{f,i}$ for TBLs at supercritical pressure with $T_w/T_\infty = 4$ and 8 deviates from the proposed skin-friction scaling law, with errors ranging from 9.7 % to 16.7 %. This is because the GFM transformation used to calculate $\overline{U}_I$ in $Re_{\theta*}$ has been shown in figure 5(*b*) to deviate from the incompressible velocity profile for these cases. Therefore, it can be concluded that the present skin-friction transformation is not suitable for TBLs at supercritical pressure and TBLs involving non-air-like viscosity laws. Researchers focusing on these flows can establish the corresponding skin-friction scaling law by using $Re_{\theta*}$ in conjunction with an appropriate velocity transformation.

References

Bernardini, M., Modesti, D., Salvadore, F. & Pirozzoli, S. 2021 STREAmS: a high-fidelity accelerated solver for direct numerical simulation of compressible turbulent flows. *Comput. Phys. Commun.* **263**, 107906.

Bernardini, M., Modesti, D., Salvadore, F., Sathyanarayana, S., Della Posta, G. & Pirozzoli, S. 2023 STREAmS-2.0: supersonic turbulent accelerated Navier–Stokes solver version 2.0. *Comput. Phys. Commun.* **285**, 108644.

Bradshaw, P. 1977 Compressible turbulent shear layers. *Annu. Rev. Fluid Mech.* **9** (1), 33–52.

Chen, X., Cheng, C., Gan, J. & Fu, L. 2023 Study of the linear models in estimating coherent velocity and temperature structures for compressible turbulent channel flows. *J. Fluid Mech.* **973**, A36.

Chen, X., Gan, J. & Fu, L. 2024 An improved Baldwin–Lomax algebraic wall model for high-speed canonical turbulent boundary layers using established scalings. *J. Fluid Mech.* **987**, A7.

Chen, X. & Sreenivasan, K.R. 2021 Reynolds number scaling of the peak turbulence intensity in wall flows. *J. Fluid Mech.* **908**, R3.

Cheng, C. & Fu, L. 2024 A Reynolds analogy model for compressible wall turbulence. *J. Fluid Mech.* **999**, A20.

Cogo, M., Baù, U., Chinappi, M., Bernardini, M. & Picano, F. 2023 Assessment of heat transfer and Mach number effects on high-speed turbulent boundary layers. *J. Fluid Mech.* **974**, A10.

van Driest, E.R. 1951 Turbulent boundary layer in compressible fluids. *J. Aeronaut. Sci.* **18** (3), 145–160.

Duan, L., Beekman, I. & Martin, M.P. 2010 Direct numerical simulation of hypersonic turbulent boundary layers. Part 2. Effect of wall temperature. *J. Fluid Mech.* **655**, 419–445.

Griffin, K.P., Fu, L. & Moin, P. 2021 Velocity transformation for compressible wall-bounded turbulent flows with and without heat transfer. *Proc. Natl Acad. Sci. USA* **118** (34), e2111144118.

Hasan, A.M., Larsson, J., Pirozzoli, S. & Pecnik, R. 2023 Incorporating intrinsic compressibility effects in velocity transformations for wall-bounded turbulent flows. *Phys. Rev. Fluids* **8** (11), L112601.

Hopkins, E.J. & Inouye, M. 1971 An evaluation of theories for predicting turbulent skin friction and heat transfer on flat plates at supersonic and hypersonic Mach numbers. *AIAA J.* **9** (6), 993–1003.

Huang, J., Duan, L. & Choudhari, M.M. 2022 Direct numerical simulation of hypersonic turbulent boundary layers: effect of spatial evolution and Reynolds number. *J. Fluid Mech.* **937**, A3.

Kawai, S. 2019 Heated transcritical and unheated non-transcritical turbulent boundary layers at supercritical pressures. *J. Fluid Mech.* **865**, 563–601.

Kianfar, A., Di Renzo, M., Williams, C., Elnahhas, A. & Johnson, P.L. 2023 Angular momentum and moment of total enthalpy integral equations for high-speed boundary layers. *Phys. Rev. Fluids* **8** (5), 054603.

Li, X., Tong, F.L., Yu, C.P. & Li, X.L. 2019 Statistical analysis of temperature distribution on vortex surfaces in hypersonic turbulent boundary layer. *Phys. Fluids* **31** (10), 106101.

Li, X.L., Fu, D.X., Ma, Y.W. & Gao, H. 2009 Acoustic calculation for supersonic turbulent boundary layer flow. *Chin. Phys. Lett.* **26** (9), 094701.

Maeyama, H. & Kawai, S. 2023 Near-wall numerical coherent structures and turbulence generation in wall-modelled large-eddy simulation. *J. Fluid Mech.* **969**, A29.

Marusic, I. & Monty, J.P. 2019 Attached eddy model of wall turbulence. *Annu. Rev. Fluid Mech.* **51** (1), 49–74.

Marusic, I., Monty, J.P., Hultmark, M. & Smits, A.J. 2013 On the logarithmic region in wall turbulence. *J. Fluid Mech.* **716**, R3.

Nagib, H.M., Chauhan, K.A. & Monkewitz, P.A. 2007 Approach to an asymptotic state for zero pressure gradient turbulent boundary layers. *Phil. Trans. R. Soc. A: Math. Phys. Engng Sci.* **365** (1852), 755–770.

Pirozzoli, S. 2011 Numerical methods for high-speed flows. *Annu. Rev. Fluid Mech.* **43** (1), 163–194.

Pirozzoli, S. & Bernardini, M. 2011 Turbulence in supersonic boundary layers at moderate Reynolds number. *J. Fluid Mech.* **688**, 120–168.

Samie, M., Marusic, I., Hutchins, N., Fu, M.K., Fan, Y., Hultmark, M. & Smits, A.J. 2018 Fully resolved measurements of turbulent boundary layer flows up to $Re_\tau = 20\,000$. *J. Fluid Mech.* **851**, 391–415.

Schlatter, P. & Örlü, R. 2010 Assessment of direct numerical simulation data of turbulent boundary layers. *J. Fluid Mech.* **659**, 116–126.

Sillero, J.A., Jiménez, J. & Moser, R.D. 2013 One-point statistics for turbulent wall-bounded flows at Reynolds numbers up to $\delta^+ \approx 2000$. *Phys. Fluids* **25** (10), 105102.

SMITS, A.J., MATHESON, N. & JOUBERT, P.N. 1983 Low-Reynolds-number turbulent boundary layers in zero and favorable pressure gradients. *J. Ship Res.* **27** (3), 147–157.

SMITS, A.J., MCKEON, B.J. & MARUSIC, I. 2011 High–Reynolds number wall turbulence. *Annu. Rev. Fluid Mech.* **43** (1), 353–375.

SPALDING, D.B. & CHI, S.W. 1963 Skin friction exerted by a compressible fluid stream on a flat plate. *AIAA J.* **1** (9), 2160–2161.

SPALDING, D.B. & CHI, S.W. 1964 The drag of a compressible turbulent boundary layer on a smooth flat plate with and without heat transfer. *J. Fluid Mech.* **18** (1), 117–143.

TRETTEL, A. & LARSSON, J. 2016 Mean velocity scaling for compressible wall turbulence with heat transfer. *Phys. Fluids* **28** (2), 026102.

VOLPIANI, P.S., BERNARDINI, M. & LARSSON, J. 2018 Effects of a nonadiabatic wall on supersonic shock/boundary-layer interactions. *Phys. Rev. Fluids* **3** (8), 083401.

VOLPIANI, P.S., BERNARDINI, M. & LARSSON, J. 2020*a* Effects of a nonadiabatic wall on hypersonic shock/boundary-layer interactions. *Phys. Rev. Fluids* **5** (1), 014602.

VOLPIANI, P.S., IYER, P.S., PIROZZOLI, S. & LARSSON, J. 2020*b* Data-driven compressibility transformation for turbulent wall layers. *Phys. Rev. Fluids* **5** (5), 052602.

ZHANG, C., DUAN, L. & CHOUDHARI, M.M. 2018 Direct numerical simulation database for supersonic and hypersonic turbulent boundary layers. *AIAA J.* **56** (11), 4297–4311.

ZHANG, P.-J.-Y., WAN, Z.-H., LIU, N.-S., SUN, D.-J. & LU, X.-Y. 2022 Wall-cooling effects on pressure fluctuations in compressible turbulent boundary layers from subsonic to hypersonic regimes. *J. Fluid Mech.* **946**, A14.

ZHANG, P.-J.-Y., WAN, Z.-H., SUN, D.-J. & LU, X.-Y. 2024 The intrinsic scaling relation between pressure fluctuations and Mach number in compressible turbulent boundary layers. *J. Fluid Mech.* **993**, A2.

ZHANG, Y.-S., BI, W.-T., HUSSAIN, F., LI, X.-L. & SHE, Z.-S. 2012 Mach-number-invariant mean-velocity profile of compressible turbulent boundary layers. *Phys. Rev. Lett.* **109** (5), 054502.